Additive Manufacturing xxx (xxxx) xxx

Contents lists available at ScienceDirect

Additive Manufacturing

journal homepage: www.elsevier.com/locate/addma

Research Paper

4D printing of patterned multimaterial magnetic hydrogel actuators

Julia Simińska-Stanny [a], Martyna Nizioł [a], Patrycja Szymczyk-Ziółkowska [b], Malwina Brożyna [c], Adam Junka [c], Amin Shavandi [d], Daria Podstawczyk [a,*]

[a] Department of Process Engineering and Technology of Polymer and Carbon Materials, Faculty of Chemistry, Wroclaw University of Science and Technology, Norwida 4/6, 50-373 Wroclaw, Poland
[b] Center for Advanced Manufacturing Technologies (CAMT/FPC), Faculty of Mechanical Engineering, Wroclaw University of Science and Technology, Łukasiewicza 5, 50-371 Wroclaw, Poland
[c] Department of Pharmaceutical Microbiology and Parasitology, Wroclaw Medical University, Borowska 211a, 50-556 Wroclaw, Poland
[d] BioMatter Unit – École Polytechnique de Bruxelles, Université Libre de Bruxelles (ULB), Avenue F.D. Roosevelt 50, CP 165/61, 1050 Brussels, Belgium

ARTICLE INFO

Keywords:
Additive manufacturing
Biocompatibility
Magnetic nanoparticles
Graded materials
Magnetic hydrogels

ABSTRACT

This paper demonstrates a new class of printable magnetic hydrogels that can be successfully used for multimaterial direct ink printing (4D printing) of soft actuators. To date, most reports on magnetic actuation have not considered biocompatibility issues associated with magnetic materials and synthetic polymers. For this reason, in this study, considerable attention was given to developing bionanocomposites that exhibit noncytotoxicity and biocompatibility and hence may be used in biomedical applications. Three inks with various concentrations of magnetic nanoparticles (MNPs) were used to print 3D objects, such as tubes (wheels), cubes, and cantilevers. The interactions between MNPs and hydrogel precursor network accounted for excellent shear thinning properties of the inks. Usually, hydrogel actuators move or change a shape upon anisotropic swelling and deswelling, possible only in an aqueous environment. Our study addresses this challenge by incorporating magnetic nanoparticles into the hydrogel, allowing for contactless in-air control of hydrogel motion. Because of the high structural integrity of the hydrogel, we can state that multimaterial direct ink printing is an excellent method for obtaining a 3D construct of high resolution, shape fidelity, tunable distribution of MNPs, and induced macroscopic anisotropy. The magnetic hydrogels are not only highly porous and noncytotoxic towards fibroblasts but also exhibit good mechanical stability and unique magnetic responsiveness. The simple approach allowed us to fabricate different magnetic actuators with various patterns, composed of magnetic and non-magnetic materials. The results demonstrate the interplay between magnetic and nonmagnetic hydrogels that influences the actuation performance of multimaterial objects, as illustrated by magnetically induced rolling, jumping, and bending. It was shown that programmable patterning of the hydrogels leads to the development of macroscopically anisotropic magnetic material. Our study confirmed that the intersection of 4D printing of magnetically responsive hydrogel materials and programmable patterning promises to fulfill future soft robotics' biocompatibility and functionality requirements.

Abbreviations: ALG, sodium alginate; MAPs, magnetoactive particles; MC, methylcellulose; MNPs, magnetic nanoparticles; NPs, nanoparticles; P0, nonmagnetic hydrogel consisting of one-type ink (contains 0% magnetic nanoparticles); P10, magnetic hydrogel consisting of one-type ink (contains 10% magnetic nanoparticles); P20, magnetic hydrogel consisting of one-type ink (contains 20% magnetic nanoparticles); PAA, polyacrylic acid; PG, hydrogel assembled from 3 inks (thirteen layers of 0% MNPs, thirteen layers of 10% MNPs and fourteen layers of 20% MNPs); PG0, hydrogel assembled from 3 inks, measuring the bending angle for the cantilever where the magnet was on the side of the layers with 0% MNPs; PG20, hydrogel assembled from 3 inks, measuring the bending angle for the cantilever where the magnet was on the side of the layers with 20% MNPs; PL, hydrogel consisting of two-type inks altered after every two deposited layers; PW, hydrogel consisting of two-type inks altered after every ten deposited layers; PW10, hydrogel consisting of two-type inks that were altered after every ten deposited layers (ten layers of 0% MNPs, ten layers of 10% MNPs, etc.); PW20, hydrogel consisting of two-type inks that were altered after every ten deposited layers (ten layers of 0% MNPs, ten layers of 20% MNPs, etc.); PL10, hydrogel consisting of two-type inks that were altered after every two deposited layers (ten layers of 0% MNPs, ten layers of 10% MNPs, etc.); PL20, hydrogel consisting of two-type inks that were altered after every two deposited layers (ten layers of 0% MNPs, ten layers of 20% MNPs, etc.); SPIONs, superparamagnetic iron oxide nanoparticles; UW, ultrapure water.

* Corresponding author.
E-mail address: daria.podstawczyk@pwr.edu.pl (D. Podstawczyk).

https://doi.org/10.1016/j.addma.2021.102506
Received 10 September 2021; Received in revised form 27 October 2021; Accepted 19 November 2021
Available online 25 November 2021

1. Introduction

Stimuli-responsive hydrogels and composites have evolved as soft materials with promising applications in several fields, including electronic devices [1,2], sensors [3], soft robots [4], and actuators [5,6]. Biopolymeric gels have gained significant attention largely owing to their excellent biocompatibility and high water capacity [7,8]. However, their actuation is usually driven by slow volume changes upon anisotropic swelling and deswelling, requiring an aqueous environment [9]. Magnetoactive particles (MAPs) may serve as an effective filler of hydropolymers to introduce remote and contactless actuation in water and air [10,11]. These MAPs include ferrites, superparamagnetic iron nanoparticles, or neodymium particles. Nanocomposites of polymers (elastomers and hydrogels) and MAPs exhibit exceptional magnetic responsive features, such as the temporal deformation without fracture upon exposure to a magnetic field [12–14]. Most magnetically responsive materials, especially those containing neodymium particles and elastomers, remain nonbiocompatible and nonbiodegradable despite their magnetic properties [15–17].

A key factor in developing soft robots for biomedical applications is the biocompatibility of robotic materials [18]; therefore, significant attention has been dedicated to replacing synthetic materials with biopolymeric alternatives. Biocomposites of magnetite nanoparticles and hydrogels are an auspicious class of biocompatible and stimuli-responsive materials for soft robotics [19–21].

Several strategies have been developed to introduce nanoparticle anisotropy into polymeric materials, such as nanoparticles (NPs) and controlled diffusion within the matrix driven by external stimuli [22]. For example, externally applied magnetic fields were used to pattern agarose hydrogels with a gradient of growth factor-linked MNPs to induce osteogenesis [23]. In another approach, gold ions diffused across the 3D polymer matrix to form an ionic gradient followed by the in situ reduction of ions to nanoparticles [24].

The strategies mentioned above fail to produce more complex patterns. 3D printing (additive manufacturing) provides an excellent, systematic tool to create programmed multimaterial designs. Recently, multimaterial 3D printing has been capturing attention because it enables the integration of multiple materials into one 3D object in a single printing process [25,26]. When combined with stimuli-responsive polymers, additive manufacturing transforms into 4D printing by employing an extra time dimension compared to traditional 3D printing [27–29]. The capability of 4D objects to change their shape over time in response to an environmental stimulus has been beneficial for various soft robotic and actuating systems [13,30]. Current hydrogel actuators can exhibit motions such as bending [31], jumping [32–34], folding [35], walking [36], swimming [37,38], rolling [39], and cargo transporting [40]. For example, Xiang et al. developed photoinduced polyurethane actuators, whose motion depended on the shape and irradiation position [41]. Upon irradiation, their photodriven hydrogel wheels rolled forward and backward, and biomimetic hydrogel flowers blossomed out. Usually, UV- or laser-based techniques such as digital light processing (DLP) and stereolithography (SLA) are used to fabricate soft actuators [42–45]. Being different from DLP and SLA, direct ink printing creates 3D structures by directly extruding shear-thinning inks [25,46,47]. In recent years, 4D direct ink printing has emerged as a fast and straightforward technique to fabricate various hydrogel actuators and robots [31,48]. However, reports on multimaterial 4D direct ink printing have been limited to the last few years [49–51]. First attempts to 3D print magnetically active hydrogel structures have been made only recently [52–54]. For example, Chen et al. fabricated a hydrogel octopus with UV-cured hydrogel precursor blended with commercial MNPs [54]. The magnetic soft robot was capable of traveling on the XY plane under the driving force of the magnetic field.

Recently, patterned and gradient materials with unique properties and functionalities are catching attention. Among them, Functionally Graded Materials (FGMs) represent a new class of materials whose peculiarity concerns composition, but also microstructure and porosity, changing gradually along one or more spatial directions and resulting in a gradual change of the properties and function in such a material [55,56]. The tissues of the human body are naturally endowed with anisotropy, which allows for variations in their chemical, physical or biological properties. Due to this functional gradation of paramount importance, biomimetic or bioinspired materials are more and more often challenged to recapitulate this property of native tissues [52]. Artificial FGMs can be fabricated by a variety of methods, however, sharing a hurdle maintaining high resolution or layers' adherence. As a new technology that provides a high degree of control over spatial resolution, additive manufacturing has gained popularity. 3D printing technology, as it involves the deposition of single layers of one or more materials, enables local control of composition and microstructure in simultaneously multiple dimensions. In this way, the process conditions can be suited for the fabrication of complex FGMs with their multidimensional and directional character. Tognato R. et al. [52] have shown that hydrogel materials with a structural gradient can provide cell guidance. The cells arranged themselves along the fibers made of MNPs – containing material. The study also demonstrated that anisotropic materials can stimulate cell differentiation, which may be a promising direction for further research and a great inspiration for tissue engineering. Another breakthrough application of microscale soft devices composed of anisotropic materials could be easy navigation and controllable stimulation e.g. during Minimally Invasive Surgeries (MIS) and targeted therapy [57,58]. Gradient scaffolds could elicit different responses to a stimulus and thus create structures able to transport cargo, deliver drugs or move in a controllable way [59]. Engineering of structures with functional gradients is likely to expand the spectrum of 3D printing applications beyond the creation of structures composed of a single type of material. This should also meet the requirements of tissue engineering emphasizing the tremendous importance of the anisotropic nature of biologically inspired materials [58].

Herein, we demonstrated a novel 4D printing strategy to fabricate patterned magnetic hydrogel structures from natural polymers. The magnetic inks are mainly composed of alginate (ALG), methylcellulose (MC), and polyacrylic acid (PAA)-stabilized magnetite nanoparticles of Fe_3O_4 (MNPs), as shown in Fig. 1.1. Three inks with different magnetic filler concentrations (Fig. 1.2) were prepared and used to print (Fig. 1.3) 3D shapes such as tubes (wheels), cubes, and cantilevers. Programmable patterning of the hydrogels led to the development of macroscopically anisotropic magnetic material. When subjected to a magnetic field, the printed objects exhibited different shape- and pattern-dependent magnetic responses, including rolling, jumping, and bending (Fig. 1.4). To our knowledge, this is the first demonstration of the multimaterial 4D printing of patterned magnetic hydrogel actuators.

2. Experimental section

2.1. Synthesis of PAA-stabilized magnetite NPs

The suppliers of the chemicals used in this work are summarized in Supplementary material. Magnetite magnetic nanoparticles (Fe_3O_4) were synthesized via the coprecipitation technique according to a protocol proposed by Ravikumar and Bandyopadhyaya [60] with some modifications as described in our previous study [53]. Accordingly, an aqueous (ultrapure water) solution of Fe^{2+} and Fe^{3+} with a Fe^{2+}/Fe^{3+} molar ratio of 1/2 was prepared to obtain iron nanoparticles. Mixing the components was carried out at a temperature of 80 °C and a nitrogen atmosphere to avoid uncontrolled oxidation of iron(II) and (III) ions. Five milliliters of ammonium hydroxide (25% solution) was added to the mixture in the next step. After 10 min, polyacrylic acid sodium salt (PAA) was introduced to prevent the aggregation of nanoparticles in the solution. A concurrent solution blackening indicated the formation of magnetic nanoparticles. The mixing process (200 rpm) lasted for approximately an hour, and then the solution was cooled down for

30 min and dialyzed for one week in ultrapure water to remove chloride ions. The mixture was washed several times with ultrapure water and decanted to obtain ferrofluid (pH ~ 7). The nanoparticles obtained from the synthesis are described as sample MNPs and further used for magnetic ink preparation.

2.2. Preparation of magnetic and non-magnetic inks

Three types of inks differing in the content of MNPs (0%, 10%, and 20%) were prepared for the study. Inks were based on alginate and methylcellulose – ALG/MC (weight ratio of 1/1). Neutral (0%) ink was formulated by adding powdered sodium alginate to ultrapure water (UW) to obtain an 8% solution. The alginate suspension was magnetically stirred (300 rpm) while adding calcium chloride ($CaCl_2$ 6 mg/ml) in a UW/Ca^{2+} volume ratio of 3/1, followed by heating (80 °C) and adding powdered methylcellulose in a weight ratio to alginate of 1/1. The mixture was continuously stirred during the whole procedure and later ultrasonicated in a water bath for 15 min to attain homogeneity. The final pH of the 0% ink was ~6.00. Magnetic inks (10%, 20%) were prepared using the modified previously reported [53,61,62]. For preparing 10% and 20% inks, 10% or 20% ferrofluid solutions were used instead of UW. A 10% MNP solution was prepared by adding 10 ml of UW per 1 g of synthesized MNPs. ALG, MC, and $CaCl_2$ were added with the proportions established for neutral ink. The 20% ink preparation process was analogous. The pH value of both 10% and 20% inks was ~ 6.30. Eventually, three prepared inks varying in MNP content denoted as 0%, 10%, and 20%, were cooled down, first in a water bath and then in a refrigerator (~ 8 °C).

2.3. 4D printing

Hydrogel structures were printed using a BioX 3D printer (CELLINK, Sweden). The inks were prepared using the methodology previously reported [39,53]. In brief, 3 ml plastic syringes were filled with hydrogel precursors and kept overnight at ~ 8 °C. Afterward, they were centrifuged (5800 rpm) for 15 min before printing to eliminate air bubbles. Cartridges loaded with magnetic inks were subjected to the magnetic field for 20 min before printing for the magnetic arrangement of incorporated MNPs. The 3D designs (Solidworks®) were exported to an STL file and then imported into the printer software. Printing conditions (pressure, speed, and nozzle type) were optimized for each ink composition (Table S1, Supplementary material).

The 3D printing process began with loading the cartridge into a printhead. Then, the ink was pneumatically extruded through the syringe at optimized printing conditions and room temperature. Layers were deposited along the designed path on a Petri dish. During extrusion, the stage height was adjusted to maintain proper and accurate layer deposition. Pressure settings were also tuned when necessary because of temporary nozzle clogging. However, pressure changes did not exceed 10 kPa. Once the printing procedure was complete, the 3D hydrogels were submerged in 0.5 M $CaCl_2$ solution for 24 h for Ca^{2+}-crosslinking. Subsequently, the hydrogels were washed several times with ethanol and ultrapure water and stored at ~ 8 °C. Inks' and hydrogels' characterization methods are described in detail in Supplementary material.

2.4. Magnetic actuation

A neodymium magnet (20 ×50 ×5 mm) with polarity normal to the

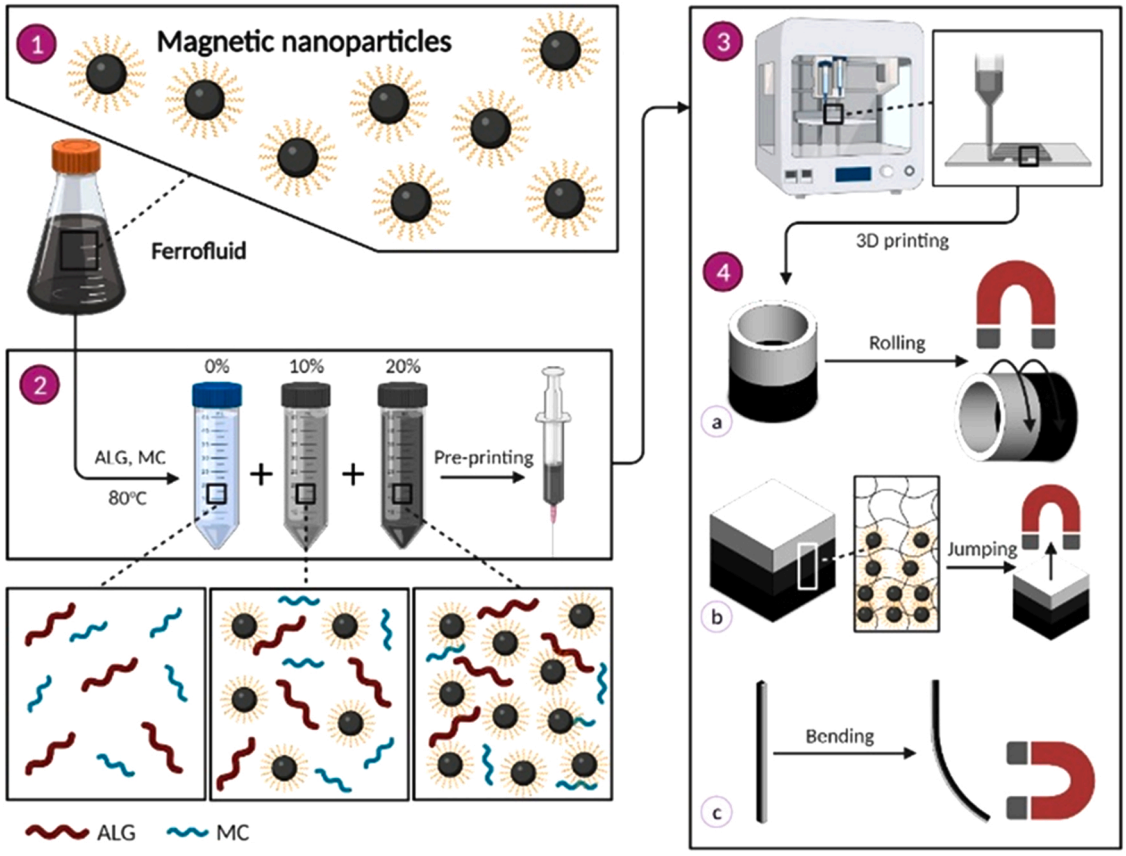

Fig. 1. Concept of the fabrication of magnetically graded materials. (1) Ferrofluid containing PAA-stabilized magnetic nanoparticles was used for the (2) preparation of magnetic inks with ferrofluid concentrations of 0%, 10%, and 20% w/w; (3) Multimaterial 3D printing of the magnetic materials; (4) Mechanism of the magnetic motions (a – rolling, b – jumping, c – bending) of the multimaterial patterned hydrogels.

plate was used to investigate the magnetic actuation of 3D-printed objects. The average magnetic field gradient observed at a 1-cm distance from the magnet was 0.2 T/cm. The strongest field of 0.23 T is present at the shorter magnet edge and decreases rapidly to values of 0.035 T and 0.015 T at distances of 1 and 2 cm from the edge surface, respectively.

The actuation approaches were dependent on the sample shape (cube, cantilever, and wheel) and pattern. All actuation tests were video recorded. Images extracted from the records were analysed in Java-based image processing and analysis software (ImageJ) to determine actuation performance. The rolling motions of the tubular samples were induced by a magnetic field applied from the bottom using a magnet moving horizontally. A magnet slowly approached its top surface for the cube specimens until the magnetic interactions were strong enough to attract the cube. Moving of the magnet towards the specimen led to its deflection in a vertical direction. Video analysis of the cube actuation allowed us to specify the height at which the magnet attracted the sample. Images of the cantilever samples were analysed using ImageJ to determine the bending angles.

3. Results and discussion

3.1. MNP characterization

The MNPs were synthesized following a previously described protocol and comprehensively characterized, ensuring that our method is reproducible for obtaining stable magnetite nanostructures. After synthesis, MNPs formed stable colloids (ferrofluid) in ultrapure water because of the stabilizing effect of polyacrylic acid (PAA). Ferrofluid and dried MNPs showed high magnetic responsiveness, as confirmed by their saturation magnetization of 60 emu/g [53]. To prevent nanoparticle cluster formation and allow anchoring to the polymeric network, MNPs were functionalized with polyacrylic acid. Upon crosslinking, calcium ions link together polyacrylic acid and alginate chains. Therefore, the hydrogel's carboxylic groups coordinate PAA-MNPs directly bounding them to the polymeric backbone [63].

Fig. 2 demonstrates the FTIR spectrum and XRD pattern of PAA-stabilized MNPs, showing the characteristic peaks of PAA-Fe_3O_4. The XRD plot (Fig. 2.1) exhibited standard diffraction reflections for magnetite at 2θ ~ 30°, 36°, 43°, 54°, 57°, 63°, 71°, and 75°, corresponding to the (220), (311), (400), (422), (511), (440), (620) and (533) planes, respectively. The analysis of the MNPs using ATR-FTIR spectroscopy shows the presence of groups originating from both magnetite

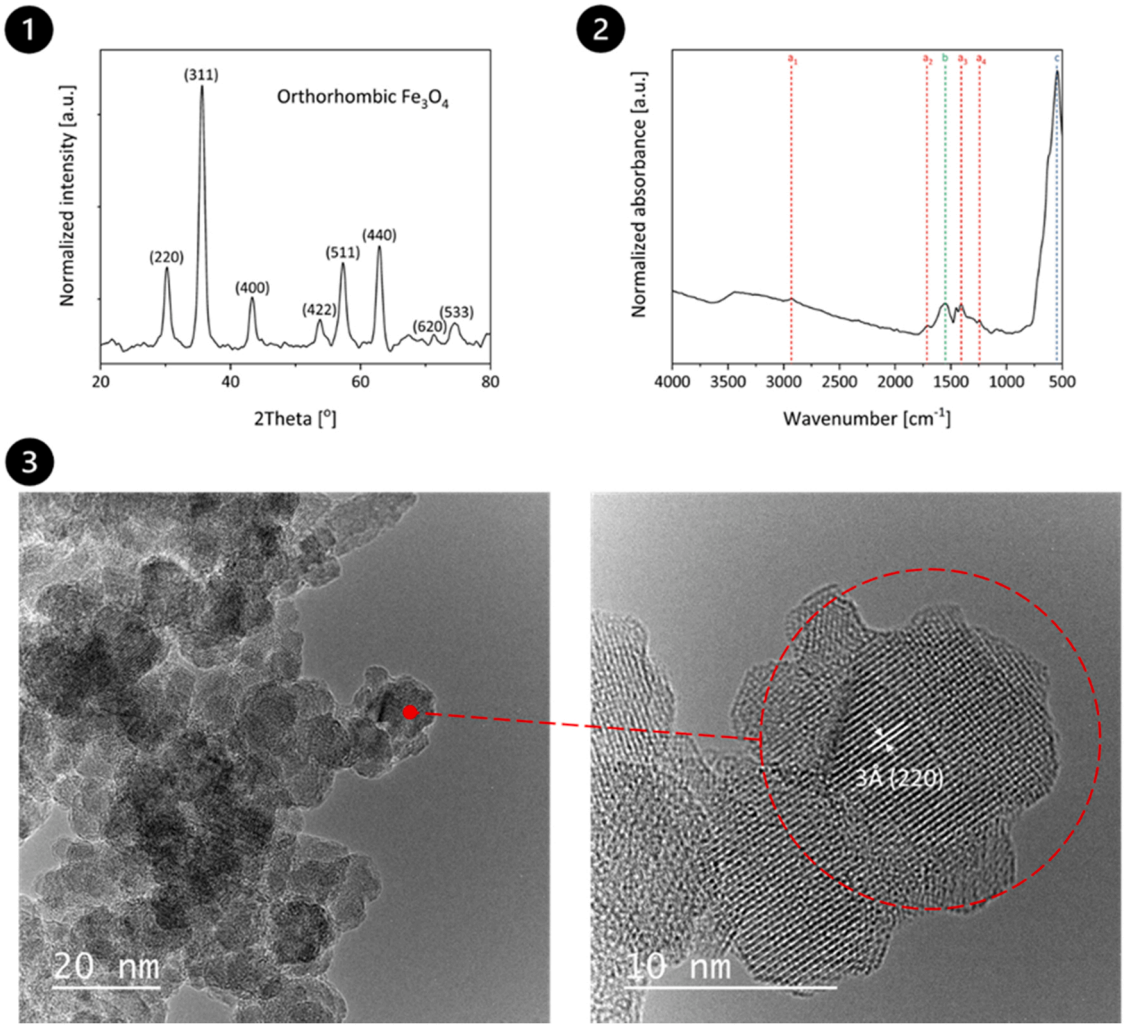

Fig. 2. Magnetic nanoparticle characteristics. (1) XRD pattern of PAA-stabilized MNPs confirming the presence of orthorhombic Fe_3O_4 in the sample. (2) The ATR-FTIR spectrum of PAA-MNPs shows peaks that correspond to the stabilizer (a1 – 2925 cm-1, a2 – 1709 cm-1, a3 – 1401 cm-1, a4 – 1241 cm-1), nanoparticles (c – 548 cm-1), and the interactions between them (b – 1549 cm-1). (3) HRTEM images of PAA-stabilized MNPs demonstrate their spherical shape when observed at lower magnification. When magnified, images reveal hexagonal nanoplates characteristic of iron oxide nanostructures (Fe_3O_4) [64].

and PAA on the NP surface. As illustrated in Fig. 2.2, four peaks at 2925, 1709, 1401, and 1241 cm^{-1} were identified in the sample corresponding to C-H stretching and bending modes and stretching vibrations of C-O, C═O, and C-OH groups in PAA, respectively [65,66]. A peak at 1549 cm^{-1} corresponds to the asymmetric stretching vibration of -COOH groups that coordinate to iron ions on the nanoparticle surface, indicating the transition of COO-H in PAA to COO-Fe. A band at 548 cm^{-1} corresponding to the Fe-O vibration of Fe_3O_4 confirmed the presence of iron oxide. HRTEM images showed PAA-stabilized MNPs with spherical shapes when analysed at lower magnification. When magnified, hexagonal nanoplates were observed. The presence of lattice fringes confirmed that nanoparticles are crystalline, and the distance between these fringes of approximately 3.0 Å corresponds to the (220) planes of the Fe_3O_4 crystal (Fig. 2.3) [64], thus confirming magnetite nanostructure formation.

In a previous study [53], we demonstrated the superparamagnetic behavior of our MNPs. Superparamagnetic iron oxide nanoparticles (SPIONs) are biocompatible NPs with low aggregation when exposed to external magnetic fields [67]. Therefore, SPIONs are of great interest for developing biomedical hydrogels.

3.2. Ink rheological characterization

First rheological measurements of the magnetic inks were performed (Fig. 3). The shear-thinning behavior of the inks was achieved by incorporating methylcellulose as a rheological modifier. Hydrogen bonds form between hydroxyl groups in MC, and the interactions between the MC backbone and water molecules are responsible for forming highly viscous MC-based hydrogel networks [68]. Our previous study optimized the ALG/MC ratio to ensure the high printability and shape fidelity of the hydrogel [53]. In this paper, the rheology of inks with varying MNP contents of 0%, 10%, and 20% and constant alginate (8%) and methylcellulose concentrations (8%) was measured. The log-log rheological curves indicate viscoelastic properties of both nonmagnetic and magnetic hydrogels, because of G′ values higher than G" values at low frequencies (Fig. 3.1). Therefore, magnetic inks can be regarded as elastic within the whole measured range of frequencies (0–70 Hz) and possess excellent shear-thinning behavior.

As demonstrated in Fig. 3.1, the incorporation of magnetic nanoparticles into the inks reduced the viscoelastic moduli. This can be because of the interaction of PAA-stabilized MNPs through repulsion with hydroxyl and carboxyl groups in methylcellulose and alginate molecules, thereby reducing the hydrogen bonding within and between both polymers.

The strain sweep testing plots for the ink without MNPs exhibited a linear viscoelastic region for strains lower than 85% (Fig. 3.2). Due to the physical interaction between methylcellulose and alginate, 0% ink behaved like elastic solids at strains below 85% with a yield stress of 1380 Pa but turned to a liquid-like state at higher strains. In comparison, 10% and 20% magnetic inks had G′ values higher than G" within the ~ 0–100% and 0–150% strain regions and corresponding values of 930 and 630 Pa yield stress, respectively. Therefore, the strain sweep results suggest that magnetic nanoparticles render the nanocomposite capable of withstanding higher strains than its nonmagnetic equivalent. This phenomenon can be associated with the interaction of the MNPs with the alginate network [69] because a greater number of nanoparticles incorporated in the ink corresponds to a higher strain at the yield point.

We next calculated tanδ, which corresponds to the G"/G′ ratio. The values of tanδ were lower than 1 at the measured frequencies for all inks, suggesting their gel-like nature that was necessary for maintaining shape fidelity [70]. The shape fidelity of the materials is a feature desired for decent-quality extrusion of the inks into various 3D objects.

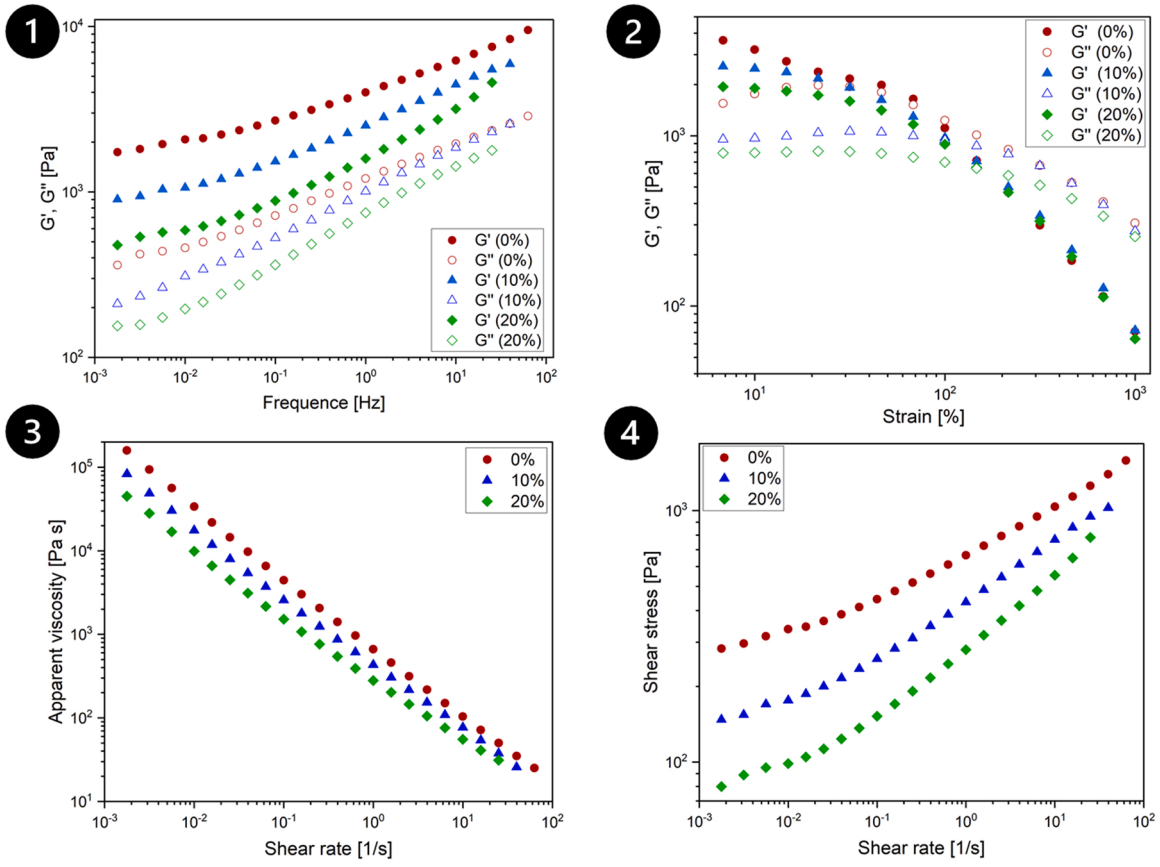

Fig. 3. Rheological properties of the individual inks (0%, 10%, and 20% w/w ferrofluid). (1) Log-log plots of storage and loss moduli vs. frequency and (2) strain (at a frequency of 1 Hz); (3) Log-log plots of the apparent viscosity of the magnetoinks; and (4) log-scale shear stress vs. shear rate plot.

The apparent viscosity was found to drastically decrease from above 10^5 Pa s for low shear rates (below 1 s^{-1}) to values lower than 10^2 Pa s and was constant until a shear rate of 60 s^{-1} was achieved (Fig. 3.3). During printing, shear stress disrupts hydrogen interactions within methylcellulose, leading to the gel-to-liquid transition. Once the shear is removed, the material quickly recovers its original gel state. Incorporating MNPs reduced shear stress due to disrupting noncovalent interactions between polymer networks (Fig. 3.4). These results suggest that printing using nonmagnetic ink induces higher shear forces within a nozzle than with its magnetic counterparts under the same printing conditions. On the other hand, interactions between magnetic nanoparticles and the hydrogel network provide increased resistance to damage under strain compared to their non-magnetic counterparts [69].

3.3. 4D printing of functionally graded structures

Here, a strategy for assembling nonmagnetic and magnetic materials in a single multimaterial 3D printing process was presented. Various objects were printed to verify the magnetic response of gradient hydrogels embedded with MNPs and illustrate their printability. Fig. S1

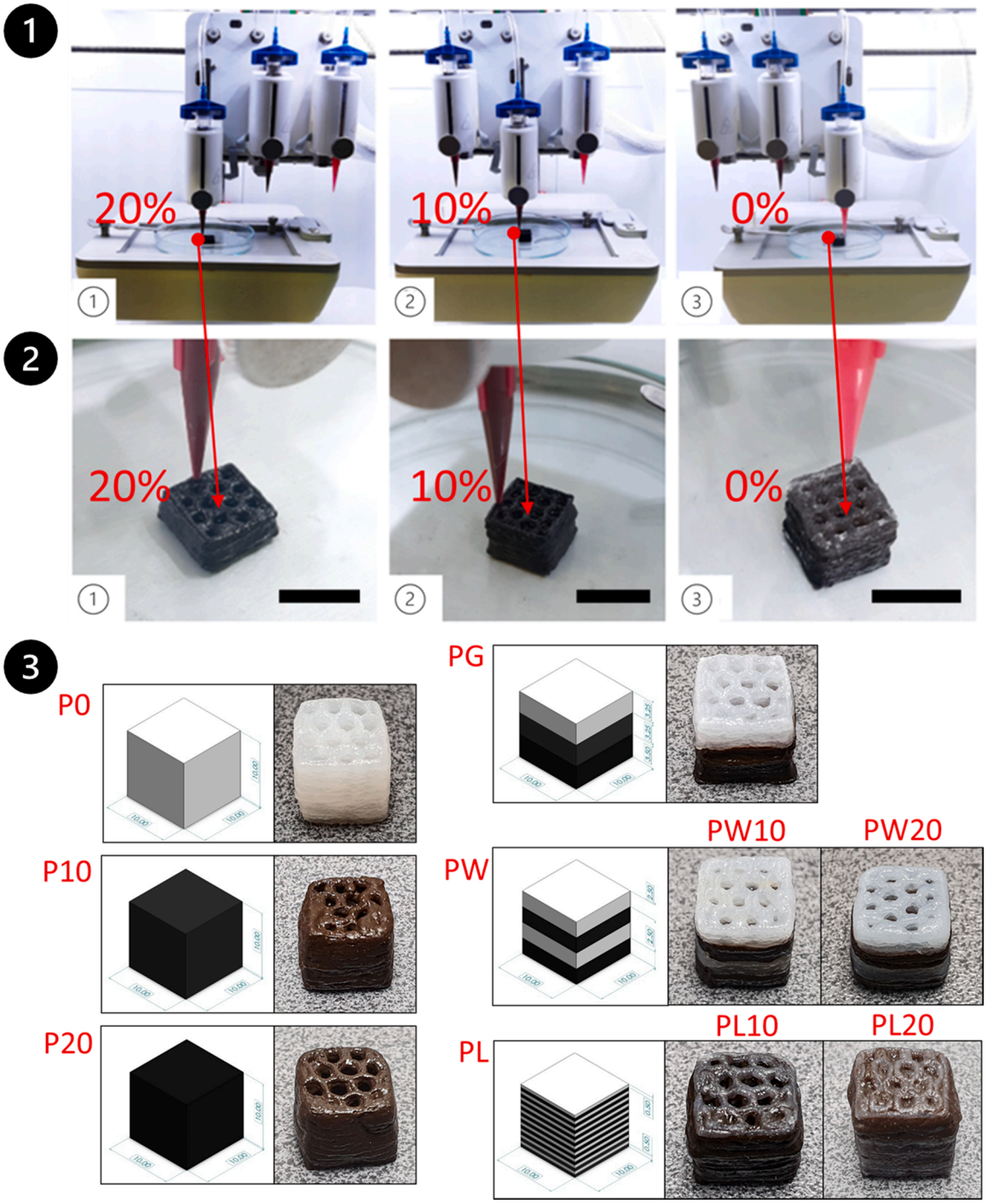

Fig. 4. (1) Multimaterial 3D printing of magnetically graded hydrogel cubes; (2) three inks with varying magnetic content were additively assembled by direct printing to form 3D nanocomposite structures; (3) various designs (left side) and print (right side) of single- and multimaterial hydrogel structure. Scale bars correspond to 1 cm.

demonstrates the fabrication of the magnetic cube (10 × 10 × 10 mm) with a gradient and shows other printouts, including hinge-type disks and tubes. Additionally, to assess the magnetic response and to prove the maneuverability of the hydrogels, magnetic cantilevers and wheels were fabricated, as presented in the following sections.

Every printing process was preceded by UV light chamber sterilization and manual printer calibration. 3D scaffolds were built layer-by-layer on Petri dishes using pneumatic extrusion. The hydrogel precursors were dispensed through a nozzle (inner diameter of 250 μm), with a printing speed of 5 mm/s and a pressure of 115–130 kPa. The 3D printer was programmed to extrude layers of different materials according to settings in g-code or directly from the printer's graphical user interface level. Such an approach allowed us to print three-dimensional structures with induced anisotropy. We focused on filament formation and uniformity upon extrusion, which was successful thanks to MNPs assembling in the magnetic field [53].

Different printing nozzles were used, either conical or cylindrical, for ink deposition. The tested diameter ranged between 200 and 410 μm. The choice for a specific nozzle depended on the required print resolution and the ability to extrude ink containing MNPs continuously. Finally, a high-precision 25 G-type nozzle (inner diameter of 250 μm) was chosen, resulting in the best print accuracy. The MNP size and rheological properties of the inks impacted the nozzle choice. Similar nozzle types were used for deposition by Sonnleitner K. et al. and our group [53,71]. To maintain the high out-of-plane stiffness of 3D printouts, we selected a honeycomb infill pattern and density of 15% for printing. Because hexagonal cell patterns have both high mechanical strength and flexibility, they can be used in motion applications, e.g., magnetic actuators [39].

To meet the challenges of multimaterial printing, a three-printhead extrusion system controlling printing material delivery was used. Depending on hydrogel composition, one to three syringes were employed (Fig. 4.1–3). Eight different cubic structures were fabricated (each group included ten hydrogels) (Fig. 4.3). The first three on the left side, described as P0, P10, and P20, consisted of one-type ink (0% or 10% or 20%), and a sample named PG was assembled from 3 inks (0%, 10%, and 20%). Samples PW and PL were printed using only two ink types: 0% and 10% (PW10 or PL10) or 0% and 20% (PW20 or PL20). Their printing process differed in the manner layers were deposited. For PW and PL, nozzles loaded with different inks were altered after every ten and two deposited layers, respectively.

Using our nonmagnetic and magnetic inks, it was also possible to print a high, dual-hydrogel 3D tube (Fig. S1) and flat hinge bending when exposed to a magnet. 3D printing experiments show that our multimaterial 3D printing via assembly of magnetic and nonmagnetic hydrogels could enable high print fidelity upon Ca^{2+} crosslinking.

Similar to Compton et al., we observed that MNPs embedded within hydrogel precursors increased ink spreading after deposition [72], specifically when compared to neutral (0%) hydrogel precursors.

Right after printing scaffold resolution was satisfactory but after soaking in ultrapure water the resolution decreased. Still, in the context of extrusion methods as direct ink writing (DIW), it should be reminded that the material swelling affects the final resolution, which is inevitable [73].

The layers from different ink types fused well together. The fusion under gravity was sufficient to assemble a 3D structure. A final magnetically graded printout, even a heterogeneous structure, was neither delaminated nor collapsed, while the layers stuck together (Fig. S2.1).

3.4. Hydrogel characterization

Next, the hydrogels' biological, structural, and mechanical properties were evaluated using cytotoxicity assays and SEM imaging, and compression tests. The interplay between magnetic and nonmagnetic materials and its effect on actuation were determined based on the results.

Unlike other magnetic nanocomposites, hydrogels with intrinsic magnetic properties have demonstrated considerable biocompatibility with various cell lines [74–76]. However, most of their applications referred to magnetized hydrogels for tissue growth induction. A great advantage of magnetic hydrogels is that they undergo magnetically driven spatial deformation resulting in stimulation of encapsulated or seeded cells [77]. When considering magnetic materials for soft robotics, their cytotoxicity evaluation is essential for applications that come into contact with body or body fluids.

To test the cytocompatibility of our printed magnetic and nonmagnetic hydrogels, in vitro viability assays using L929 fibroblasts were performed (Fig. 5.1). Cells maintained 97.6 ± 7.5% viability after 24 h when cultured with P0 based on normative neutral red (NR) uptake. In contrast, fibroblasts cultured with magnetic hydrogels exhibited cell viability above 85% in all cases compared with the positive control (100% viability). There were no statistical deviations among the tested samples and the control, demonstrating that our hydrogels are biocompatible with the tested fibroblasts.

In our previous study, we observed magnetically stimulated alignment of the hydrogel using SEM. Here, the MNP gradient along the sample height was evaluated to determine whether it influences the intrinsic structure of multimaterial hydrogels. Figs. 5.2–5 and S2.2 show the SEM images of the cross-section of the magnetically graded cantilever and cubes. The cantilever and cube consist of three layers with different amounts of MNPs (20%, 10% and 0%). All layers are stuck together with no space between them to generate a stable, cohesive object. SEM images of the hydrogel cross-section (Figs. 5.3,4 and S2.2) showed magnetic nanoparticles as bright dots well dispersed in the hydrogel structure. The MNP amount decreases with the cantilever height, and nanoparticles are absent in the bottom layer. The magnetic nanoparticles formed small, well-dispersed clusters throughout the hydrogel matrix (Fig. S2.2,). No strong aggregation was observed, suggesting that the nanoparticles were electrostatically stabilized through PAA, calcium ions, and alginate interactions [78,79]. As expected, a closer inspection of SEM images of the nanoparticle clusters (Fig. S2) demonstrated different MNP concentrations in the top (20%) and middle (10%) layers. The formation of this nanoparticle gradient was enhanced because MNPs contributed to the crosslinking of the alginate network. Strong interactions with the polymer chain locked them within the matrix and preserved the concentration gradient formed via additive manufacturing. The green line in Fig. 5.3–4 shows the transition between the magnetic (10%) and the non-magnetic layers (0%). The difference was clearly indicated by the white dots that correspond to the magnetic nanoparticles and were only present within the magnetic layer. The same magnetic-to-nonmagnetic change can be observed in the higher-magnification SEM image of the gradient cube (Fig S2.2).

The hydrogel network exhibited porous intrinsic morphology with open and closed elongated mesopores (Fig. 5.5, highlighted in yellow) with a pore diameter ranging between 4 and 16 μm. The pore distribution (Fig. 5.5, examples highlighted in green) was calculated based on 100 diameters using ImageJ. The top, middle, and bottom layer average pore sizes were 8.11 ± 2.79, 8.00 ± 2.27, and 7.85 ± 2.73 μm, respectively. These results suggest that MNPs did not significantly affect pore size and morphology; rather they influenced the surface topography. The nonmagnetic alginate layer showed a smooth polymeric surface (Fig. S2.2.1) compared to the rough surface of the MNP layers (Fig. S2.2.3)). Similar differences between nanoparticle-loaded and nanoparticle-less polymer structures were reported in previous papers by our group and other researchers [53,80,81]. Finally, we compared the hydrogel porosity alongside its width. The left side (Fig. 5.3) exhibited a denser structure than the middle part (Fig. 5.4), and the pore size increased from left to right. The hydrogel walls were directly in contact with calcium chloride during crosslinking, while the center was crosslinked by Ca^{2+} diffusion [82,83]. As a result, the Ca^{2+}-exposed side has a higher crosslinking density than the center. The other explanation

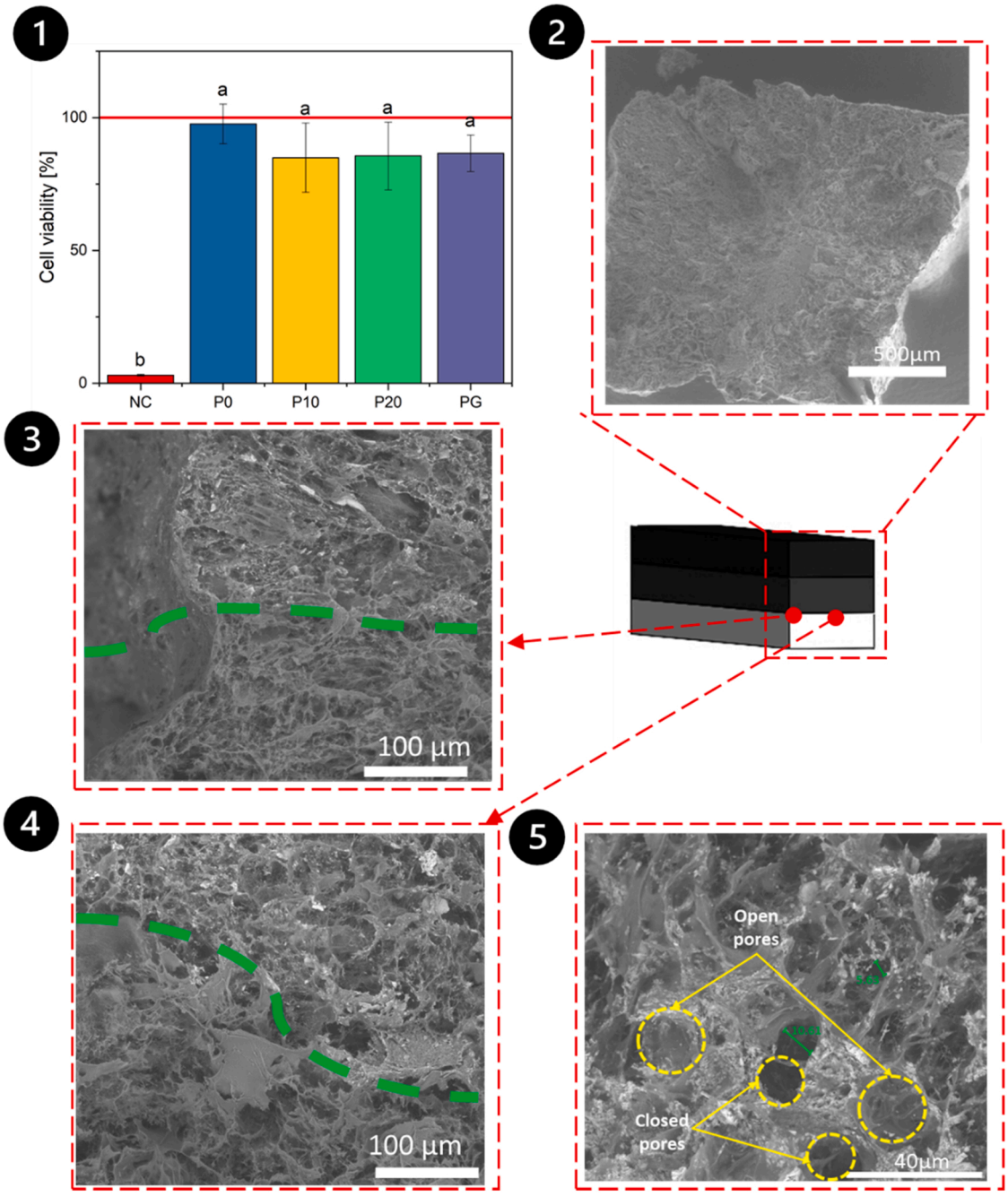

Fig. 5. (1) L929 fibroblast viability incubated with hydrogel extracts and ethanol (negative control, NC). The red solid line corresponds to a positive control (100%); (2) SEM overview of the sample and scheme of the cross-section of the cantilever showing the functional gradient; (3) SEM images of the left side and the center (4) of the cantilever between a layer containing 10% MNPs and a non-magnetic layer (the green line shows the border of the layers) (5) SEM image showing the pore type (yellow) diameters (green). (For interpretation of the references to color in this figure legend, the reader is referred to the web version of this article.)

for the differences between the outer and middle structures may be the nonuniform heat transfer during the freeze-drying process [84]. Consequently, the freezing effect is stronger on the sample surface than in its interior.

Next, we determined the mechanical properties of the printed cubic hydrogels containing different patterns of magnetic and nonmagnetic layers (Fig. S2.3) via a static compression test. Mechanical experiments aimed to evaluate the relationship between the mechanical properties and the hydrogel composition and 3D arrangement. The compressive strength (Rm) and Young's modulus (E) results are shown in Fig. 6.1 and 6.2, respectively. Because the samples did not break during the test, compressive stress at 75% strain was used.

First, the mechanical properties of single material hydrogel cubes were compared. The highest Rm (0.28 ± 0.12 MPa) was achieved for the P20 series consisting of one-type 20% ink. A decrease in the content of MNPs in the single-material hydrogel cubes resulted in a significant reduction in the mechanical properties. In particular, the compressive strength decreased to 0.25 ± 0.05 and 0.18 ± 0.05 MPa for 10% and 0% MNP content, respectively. Along with the reduction of the nanoparticle content, Young's modulus increased from 8.6 ± 1.2 MPa (P20), through 11.6 ± 2.3 MPa (P10), to 17.7 ± 1.8 MPa (P0). The introduction of MNPs into the ink may weaken alginate intrachain interactions and Ca^{2+}-crosslink density after printing. Consequently, it reduces the elastic nature of magnetic hydrogels. The compressive strength

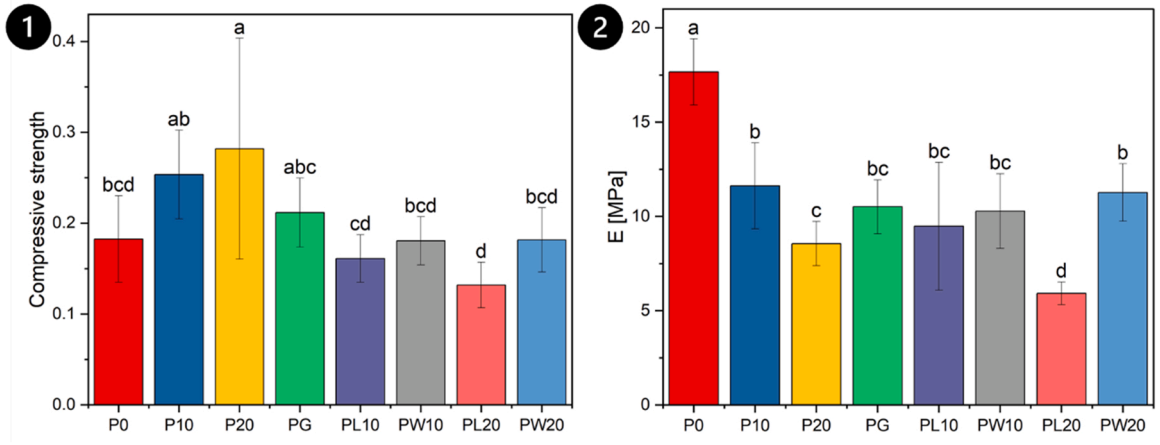

Fig. 6. Mechanical properties of the printed hydrogel cubes with different 3D patterns. (1) Compressive strength (Rm) and (2) Young's modulus (E) of the samples.

(0.21 ± 0.04 MPa) and stiffness (10.5 ± 2.0 MPa) of the magnetically graded hydrogel consisting of all three inks are between the values for single-material scaffolds (P0, P10, P20). SEM images (Fig. S2.2) showed no differences in porosity alongside the sample height. Therefore, the mechanical properties of the graded sample were due to the presence of MNPs rather than the hydrogel intrinsic structure.

The difference between PL and PW was the distribution of the layers. Numbers 10 and 20 accounted for 10% and 20% of the MNP content in the magnetic layers, respectively. The stiffness of the hydrogels in which the ink, either 10% or 0%, was changed after every two layers (PL10) was insignificantly lower (9.5 ± 3.4 MPa) than that of the sample in which the inks were altered after every ten layers (PW10) (10.3 ± 2.0 MPa). A similar trend was observed for compressive strength - 0.16 ± 0.03 MPa for PL10 versus 0.18 ± 0.03 MPa for PW10. Increasing the nanoparticle concentration up to 20% in the PL sample (PL20) reduced both E and Rm to 5.92 ± 0.61 and 0.13 ± 0.03 MPa,

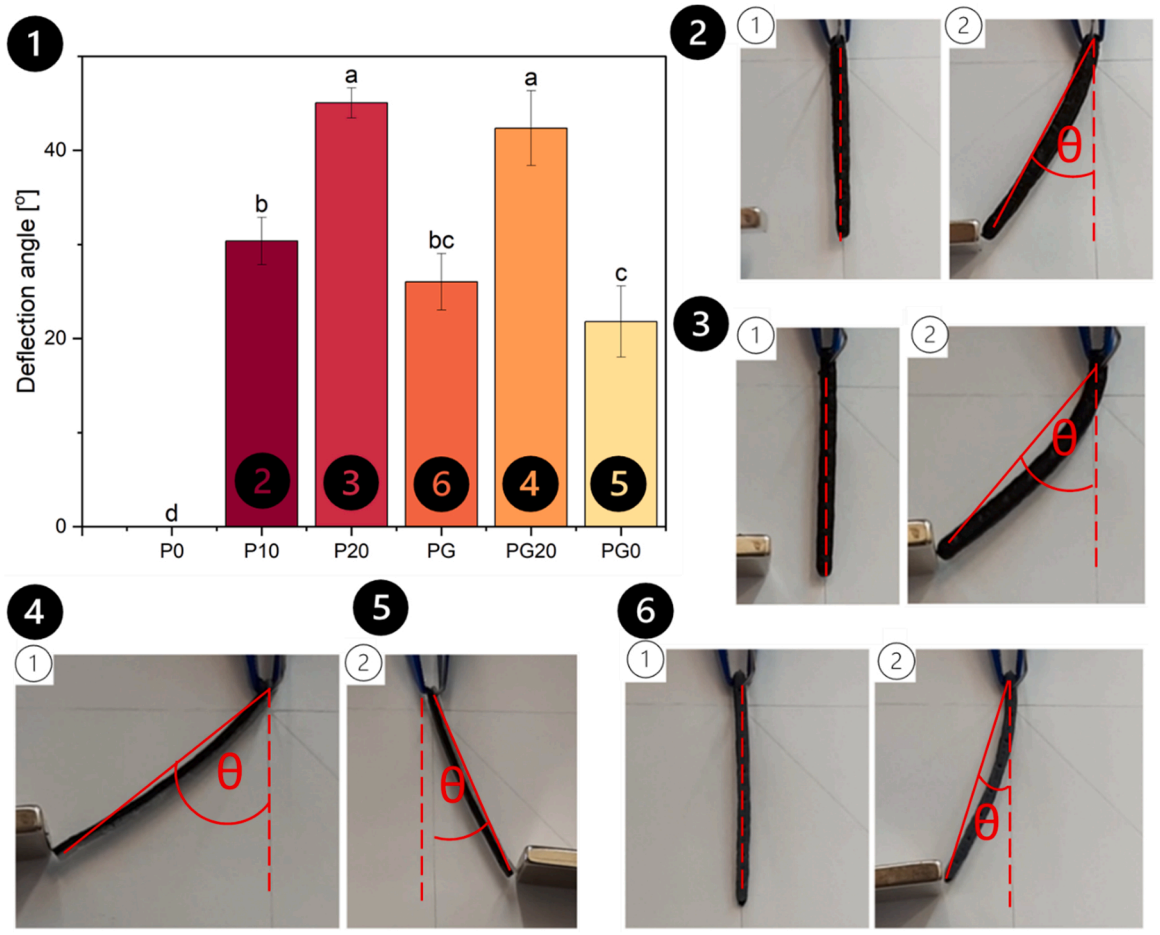

Fig. 7. 3D-printed magnetic cantilevers that bend towards the magnetic field. The bending angle strongly depends on the hydrogel composition and side exposed to a magnetic attraction. (1) The average bending angles of 3D-printed cantilevers with different three-dimensional patterns and corresponding (2–6) photos of their magnetic responses.

respectively. The hydrogels with layers being changed less frequently (PW) exhibited similar (PW10) or higher (PW20) values of Young's modulus than those of single-material samples (P10, P20). The Rm and E of PW20 were even higher than those of PW10 and reached values of 11.3 ± 1.5 and 0.18 ± 0.04 MPa, respectively. The more frequently the layers are altered, the weaker they stick together, affecting the overall mechanical stability of the multimaterial cubes.

The mechanical results suggest that the proper arrangement of magnetic and nonmagnetic layers may significantly advance the mechanical properties of the printed hydrogels and consequently the actuation. Reasonable mechanical stiffness and the good dispersion of the MNPs may allow for whole-nanocomposite movement under a magnetic field.

3.5. Actuation of the hydrogel actuator

Three magnetically responsive actuators were created: cantilevers (beams), cubes, and wheels (tubes). The samples were composed of layers of nonmagnetic and magnetic hydrogels arranged in various patterns. Samples P0, P10, and P20 were made up of one ink type at 0%, 10%, and 20%, respectively. In contrast, PG consisted magnetic gradient. Our magnetic actuators were able to move in the air upon exposure to a magnetic field. Three different motion behaviors were recorded: bending, jumping, and rolling. These movements were dependent on the 3D multimaterial patterns of the hydrogels. These findings suggest that 3D printing can introduce macroscopic anisotropy into objects.

As shown in Fig. 7, bending deformation occurs upon exposure to a magnetic field, leading to the displacement of the center of gravity of the cantilever and resulting in a range of deflection angles (Fig. 7.1). The cantilever containing 10% MNPs could bend through 30.4 ± 2.5° upon applying the static magnetic field (Fig. 7.2). The bending angle increased to 45.0 ± 1.6° when the nanoparticle content was 20% (Fig. 7.3). The graded cantilever is simply composed of several layers of magnetic and nonmagnetic hydrogels arranged in a gradient. For the gradient beams, the deflection angle differed depending on their orientation to the magnetic field. The measurements carried out in three ways showed that the strongest interaction between the magnet and the actuator occurred when the surface of the highest MNP concentration was turned in the direction of the magnet (Fig. 7.4, PG20). It led to the highest deflection angle of 42.4 ± 4.0°. When the magnet was positioned on the opposite side of the cantilever, the sample was bent by an angle of 21.8 ± 3.8° (Fig. 7.5, PG0). Sideways placement resulted in a deflection angle of 26.0 ± 3.0° (Fig. 7.6, PG). The results showed different magnetic responsiveness for the gradient beam compared to the homogenous beam, confirming the dependence of the deflection angle on the distribution of nanoparticles in the sample. As demonstrated, the gradient beam exhibited different magnetic responses depending on the sample surface exposed to the magnetic field. This unique property means that with only one actuator, we can obtain different magnetic responses with a single source of the magnetic field.

Cubic samples were compared in terms of the heights they could vertically jump when attracted by a magnet (Fig. 8.1). As expected, sample P20 demonstrated the highest jump height of 8.0 ± 1.0 mm (Fig. 8.2, Movie S1). In contrast, P10 reached a significantly lower jumping height of 3.0 ± 1.0 mm (Movie S1). Different jumping distances were achieved by controlling the gradient sample (PG) position relative to the magnet. The black side of the PG sample was elevated by 6.3 ± 0.6 mm (Movie S2). In contrast, when the cube was turned around (white side up), a distance of 0.3 ± 0.6 mm was required to lift it. A cube positioned sideways to the magnet (Fig. 8.3) rotated by 90° while jumping so that eventually, the wall parallel to the magnet surface was the one with the highest content of MNPs (Movie S2). A spatial concentration gradient led to a characteristic profile of magnetic properties and affected the actuation response [85]. Only nanoparticle gradient cubes exhibited a unique ability to rotate and jump under an external magnetic field. Because of this special property, the PG sample could be used as an intelligent hydrogel valve remotely controlled by magnetic stimulation.

Supplementary material related to this article can be found online at doi:10.1016/j.addma.2021.102506.

Next, tubes (wheels) with three different patterns (Fig. 9.1) were printed and their rolling motion was induced by applying a static magnetic field (Fig. S3.3). For this purpose, a bar magnet was placed underneath a smooth plastic surface on which the samples were actuated. The magnetic field of the bar magnet is the weakest in its center and increases towards either of its poles, where the force is equally strong. All wheel-shaped hydrogel samples were placed at the position in the middle of the length of the magnet. Therefore, they were subjected to a spatially nonuniform magnetic field. A two-part wheel (nonsymmetrical C and D samples) exhibited turning motion with a direction depending on the object's initial position relative to the magnet

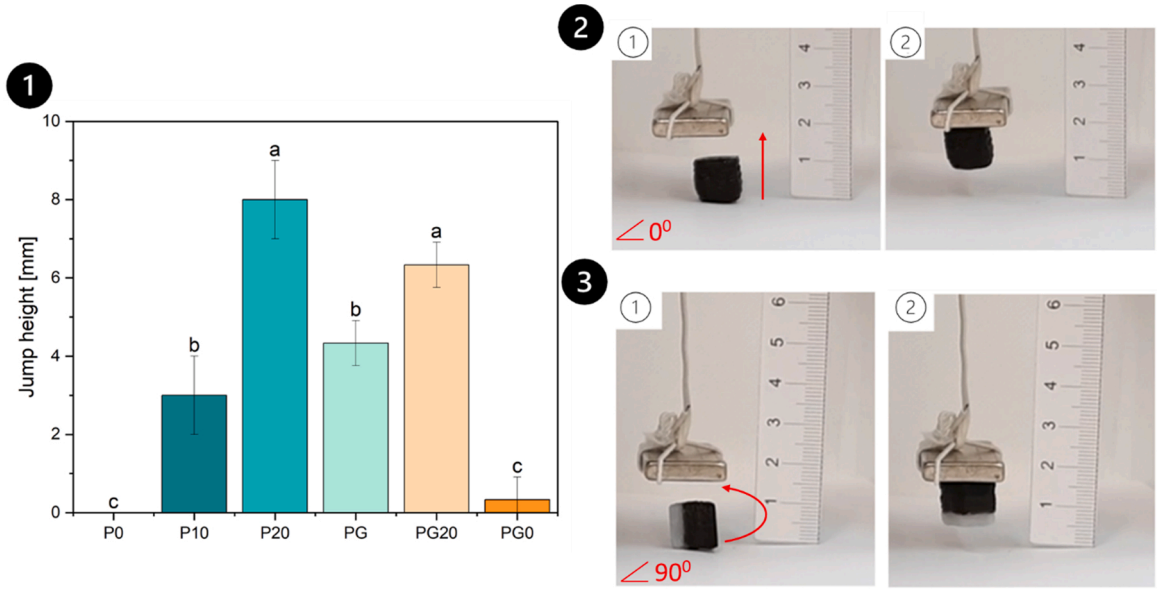

Fig. 8. Magnetic hydrogel cubes can jump up under a magnetic field. (1) Jumping heights for different 3D-printed cubes; (2) P20 can jump almost a distance of its own height (~ 8 mm); (3) PG laying on its site can rotate in the direction of the magnetic field and jump to a height of ~ 5 mm.

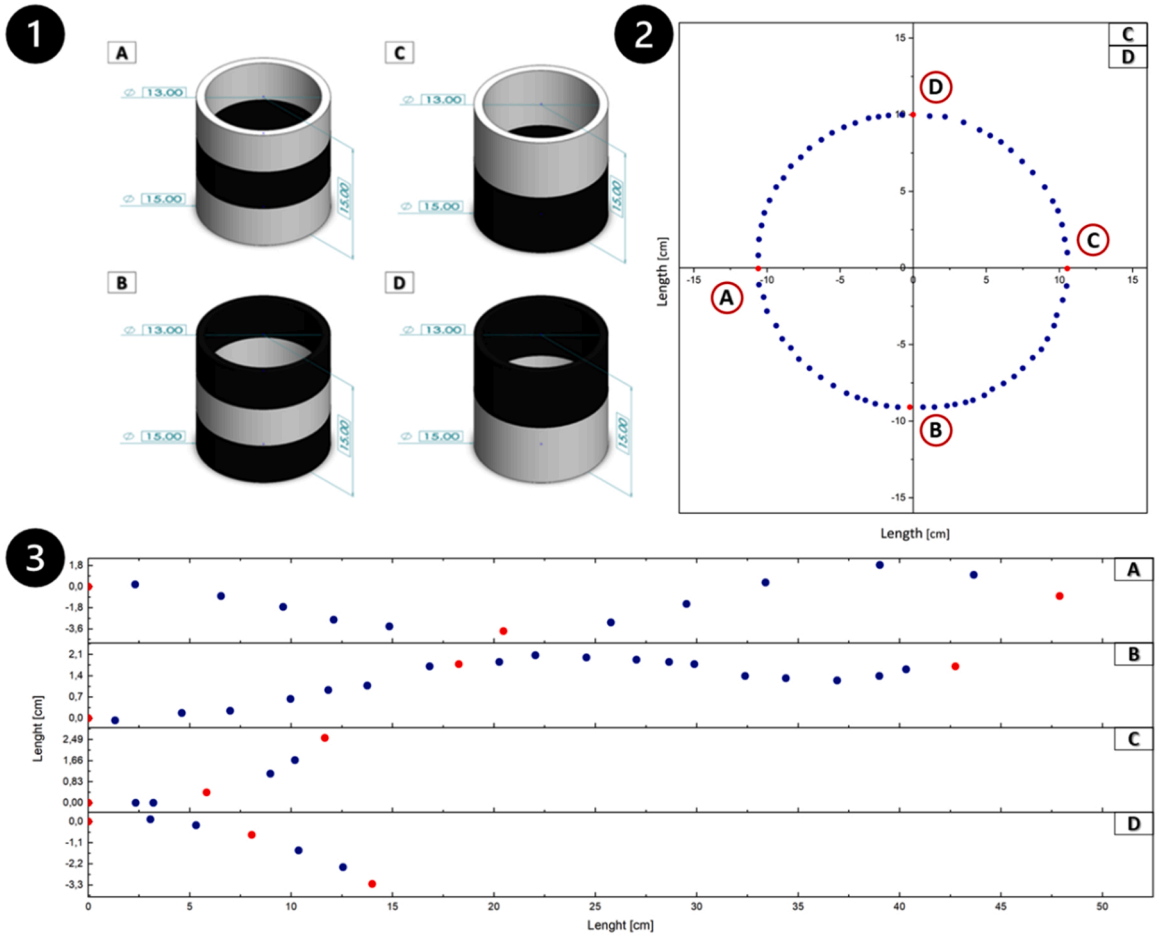

Fig. 9. Magnetic responsiveness of 3D-printed tubes (wheels). (1) Various designs of multimaterial wheels; (2)) magnetic field forces the di-material hydrogel tube (C, D) to roll along a circular path of radius ~ 10 cm. The tube could complete a full rotation from A through B and C to D; and (3) magnetic field drives the multimaterial wheels to roll along paths that depend on the object pattern, with photo labels corresponding to plots A-D.

(Fig. 9.2C, D). Because of the initial position in the middle of the magnet's length, the magnetic part of the wheel was subjected to a spatially nonuniform magnetic field. MNPs anchored to the hydrogel network interacted with the matrix so that the whole nanocomposite could move. Driven by the mechanism mentioned above, macroscopic rolling motion towards the highest field intensity was observed. Consequently, samples C and D turned at angles of 22° and 15°, respectively, after traveling a distance of ~ 15 cm. Because of its ability to turn, the two-part hydrogel tube (C, D) could roll along a circular path of radius ~ 10 cm. The tube completed a full rotation from A through B and C to D.

The symmetrical 3D pattern of tubes A and B caused magnetic parts to be equally attracted by the magnet (Fig. 9.3A, B). As a result, the three-part wheels could roll forward or backward on the smooth slab driven by the magnetic field. Slight deviations from the straight trajectory resulted from the irregular surface of the tube. The wheels could travel ~ 50 cm with (Movie S3) and without (Movie S4) cargo (a hollow plastic tube) or even upslope at an angle of 10° (Movie S5).

Supplementary material related to this article can be found online at doi:10.1016/j.addma.2021.102506.

Images demonstrating the movement of the tubes were shown in Fig. S3.1 and 3.2. These hydrogel actuators with programmable motion can be used for cargo transportation and delivery. By hydrogel patterning, we can not only control the trajectory of the wheels but also transport cargo upward over long distances.

Following the definition of materials with a functional gradient, the arrangement of layers from materials with different properties can evoke a different structure behavior in a directional magnetic field [56]. Our experiments have shown that by printing geometrically similar structures their hidden subtleties, determining magnetic response lie in the manner of the layer's arrangement. Our results proved that magnetic and nonmagnetic hydrogels can be freely integrated into patterned structures without scaffold collapsing or delamination.

The incorporation of the functional gradient into our samples gave us a great extent of scaffolds' steering possibilities. We observed that cubic, gradient-structure rotation while moving towards a magnet, could be induced by the directional application of the magnetic field (Fig. 8). Such a phenomenon has not been observed for a homogeneous cube that only jumped when a magnetic field was applied. We can speculate that this type of movement can be applied for studies on soft-material valves of great potential in soft robotics or drug delivery. Another experiment proved that the graded cantilever responds by different deflection angles depending on the side on which it is magnetically stimulated (Fig. 7). This indicates that such a structure could be used as a flow controller. The clearance of a vessel (pipe)-like structure translating into the throughput capacity could be steered by the direction of anisotropic structure deflection upon magnetic field application. The last geometry investigated in our study revealed its potential in both movement control and cargo transport (Fig. 9). Patterned wheels, depending on the magnetic and non-magnetic material arrangement, rolled and turned when a magnetic field was applied underneath. The direction in which the trajectory turned was determined by the side of the wheel containing a higher amount of MNPs. In this vision, our wheels could be used to transport light cargo, for example in sterile areas or in places where operations should not be performed manually.

Summing up, the introduction and modification of gradients elicit find different and interesting responses to the magnetic field, which might lead to different possible applications.

4. Conclusions

In conclusion, a simple method of assembling nonmagnetic and magnetic hydrogels into single constructs via additive manufacturing was demonstrated. Using multimaterial direct printing, we fabricated different magnetic actuators with various patterns. Graded and patterned 4D-printed magnetic actuators demonstrated a spatially anisotropic response to the magnetic field, allowing for steerable motion in the air. The good adhesion between the magnetic and nonmagnetic hydrogel layers allowed the creation of a wide range of patterns, including a gradient. Stabilization of MNPs by PAA ensured their good dispersion within the polymeric matrix. Because of the Ca^{2+}-based interactions between the alginate and polyacrylic acid backbones, PAA-MNPs participated in hydrogel crosslinking. Upon gelation, their entrapment within the matrix and tendency to align along the field direction (net magnetization) were responsible for the hydrogels' macroscopic response during magnetic actuation [86].

Our magnetic cantilevers showed instantaneous bending upon application of a magnetic field. The deflection angles depended strongly on the MNP content, 3D patterns, and exposure side. Magnetically graded tubes placed sideways to the magnet surface could rotate by a right angle while being actuated. The wheel-shaped hydrogels rolled in a direction dependent on the multimaterial patterns and could transport cargo over a distance of ~ 50 cm. In addition, the hydrogels that consisted of the actuators were not cytotoxic towards fibroblasts. However further biological tests are required, the results of performed cytotoxicity tests indicate the potential applicability of our soft robots in medicine and biomedical engineering, especially.

Patterning of magnetic hydrogels via additive manufacturing opens a new window for remotely controlled and navigated hydrogel actuators in the air environment. It was demonstrated that nonmagnetic and magnetic materials could be easily combined and shaped into various multimaterial objects in a single manufacturing process. This approach may inspire other scientists to design new magnetic nanocomposites and use them to obtain a wide range of actuation responses. A broad range of biomedical applications could be developed and implemented by combining biocompatible hydrogels and magneto-reactive materials.

CRediT authorship contribution statement

Julia Simińska-Stanny: Data curation, Formal analysis, Investigation, Methodology, Software, Visualization, Writing – review & editing, Writing – original draft. **Martyna Nizioł**: Investigation, Methodology, Software, Visualization, Writing – review & editing. **Patrycja Szymczyk Ziółkowska:** Investigation. **Adam Junka:** Investigation. **Malwina Brożyna**: Investigation. **Amin Shavandi**: Writing – review & editing. **Daria Podstawczyk**: Conceptualization, Formal analysis, Funding acquisition, Investigation, Methodology, Project administration, Resources, Software, Supervision, Validation, Visualization, Writing – original draft, Writing – review & editing.

Declaration of Competing Interest

The authors declare that they have no known competing financial interests or personal relationships that could have appeared to influence the work reported in this paper.

Acknowledgments

Graphical abstract was created with BioRender.com. The authors acknowledge the Polish National Science Centre, Poland [Grant number 2016/23/D/ST8/01267].

Appendix A. Supplementary material

Supplementary data associated with this article can be found in the online version at doi:10.1016/j.addma.2021.102506.

References

[1] J.R. Aggas, S. Abasi, B. Smith, M. Zimmerman, M. Deprest, A. Guiseppi-Elie, Microfabricated and 3-D printed soft bioelectronic constructs from PAn-PAAMPSA-containing hydrogels, Bioengineering 5 (2018) 87, https://doi.org/10.3390/bioengineering5040087.

[2] J.R. Aggas, S. Abasi, J.F. Phipps, D.A. Podstawczyk, A. Guiseppi-Elie, Microfabricated and 3-D printed electroconductive hydrogels of PEDOT:PSS and their application in bioelectronics, Biosens. Bioelectron. 168 (2020), 112568, https://doi.org/10.1016/j.bios.2020.112568.

[3] H. Peng, Y. Xin, J. Xu, H. Liu, J. Zhang, Ultra-stretchable hydrogels with reactive liquid metals as asymmetric force-sensors, Mater. Horiz. 6 (2019) 618–625, https://doi.org/10.1039/C8MH01561A.

[4] L. Jing, L.-Y. Hsiao, S. Li, H. Yang, P.L.P. Ng, M. Ding, T. Van Truong, S.-P. Gao, K. Li, Y.-X. Guo, P. Valdivia y Alvarado, P.-Y. Chen, 2D-Material-integrated hydrogels as multifunctional protective skins for soft robots, Mater. Horiz. 8 (2021) 2065–2078, https://doi.org/10.1039/D0MH01594F.

[5] L. Ionov, Hydrogel-based actuators: possibilities and limitations, Mater. Today 17 (2014) 494–503, https://doi.org/10.1016/j.mattod.2014.07.002.

[6] M.A.C. Stuart, W.T.S. Huck, J. Genzer, M. Müller, C. Ober, M. Stamm, G. B. Sukhorukov, I. Szleifer, V.V. Tsukruk, M. Urban, F. Winnik, S. Zauscher, I. Luzinov, S. Minko, Emerging applications of stimuli-responsive polymer materials, Nat. Mater. 9 (2010) 101–113, https://doi.org/10.1038/nmat2614.

[7] H. Guo, J. Cheng, K. Yang, K. Demella, T. Li, S.R. Raghavan, Z. Nie, Programming the shape transformation of a composite hydrogel sheet via erasable and rewritable nanoparticle patterns, ACS Appl. Mater. Interfaces 11 (2019) 42654–42660, https://doi.org/10.1021/acsami.9b16610.

[8] J.-Y. Sun, X. Zhao, W.R.K. Illeperuma, O. Chaudhuri, K.H. Oh, D.J. Mooney, J. J. Vlassak, Z. Suo, Highly stretchable and tough hydrogels, Nature 489 (2012) 133–136, https://doi.org/10.1038/nature11409.

[9] M. Li, X. Wang, B. Dong, M. Sitti, In-air fast response and high speed jumping and rolling of a light-driven hydrogel actuator, Nat. Commun. 11 (2020) 3988, https://doi.org/10.1038/s41467-020-17775-4.

[10] Q. Cao, Q. Fan, Q. Chen, C. Liu, X. Han, L. Li, Recent advances in manipulation of micro- and nano-objects with magnetic fields at small scales, Mater. Horiz. 7 (2020) 638–666, https://doi.org/10.1039/C9MH00714H.

[11] M.V. Patton, P. Ryan, T. Calascione, N. Fischer, A. Morgenstern, N. Stenger, B. B. Nelson-Cheeseman, Manipulating magnetic anisotropy in fused filament fabricated parts via macroscopic shape, mesoscopic infill orientation, and infill percentage, Addit. Manuf. 27 (2019) 482–488, https://doi.org/10.1016/j.addma.2019.03.026.

[12] J. Thévenot, H. Oliveira, O. Sandre, S. Lecommandoux, Magnetic responsive polymer composite materials, Chem. Soc. Rev. 42 (2013) 7099–7116, https://doi.org/10.1039/C3CS60058K.

[13] A. Kania, K. Berent, T. Mazur, M. Sikora, 3D printed composites with uniform distribution of Fe_3O_4 nanoparticles and magnetic shape anisotropy, Addit. Manuf. 46 (2021), 102149, https://doi.org/10.1016/j.addma.2021.102149.

[14] X. Peng, X. Kuang, D.J. Roach, Y. Wang, C.M. Hamel, C. Lu, H.J. Qi, Integrating digital light processing with direct ink writing for hybrid 3D printing of functional structures and devices, Addit. Manuf. 40 (2021), 101911, https://doi.org/10.1016/j.addma.2021.101911.

[15] V.M. Kadiri, C. Bussi, A.W. Holle, K. Son, H. Kwon, G. Schütz, M.G. Gutierrez, P. Fischer, Biocompatible magnetic micro- and nanodevices: fabrication of FePt nanopropellers and cell transfection, Adv. Mater. 32 (2020), 2001114, https://doi.org/10.1002/adma.202001114.

[16] A.C. Bakenecker, A. von Gladiss, H. Schwenke, A. Behrends, T. Friedrich, K. Lüdtke-Buzug, A. Neumann, J. Barkhausen, F. Wegner, T.M. Buzug, Navigation of a magnetic micro-robot through a cerebral aneurysm phantom with magnetic particle imaging, Sci. Rep. 11 (2021) 14082, https://doi.org/10.1038/s41598-021-93323-4.

[17] S.Y. Hann, H. Cui, M. Nowicki, L.G. Zhang, 4D printing soft robotics for biomedical applications, Addit. Manuf. 36 (2020), 101567, https://doi.org/10.1016/j.addma.2020.101567.

[18] L. Jing, K. Li, H. Yang, P.-Y. Chen, Recent advances in integration of 2D materials with soft matter for multifunctional robotic materials, Mater. Horiz. 7 (2020) 54–70, https://doi.org/10.1039/C9MH01139K.

[19] P. Ilg, Stimuli-responsive hydrogels cross-linked by magnetic nanoparticles, Soft Matter 9 (2013) 3465–3468, https://doi.org/10.1039/C3SM27809C.

[20] J. Tang, Q. Yin, Y. Qiao, T. Wang, Shape morphing of hydrogels in alternating magnetic field, ACS Appl. Mater. Interfaces 11 (2019) 21194–21200, https://doi.org/10.1021/acsami.9b05742.

[21] J. Tang, Z. Tong, Y. Xia, M. Liu, Z. Lv, Y. Gao, T. Lu, S. Xie, Y. Pei, D. Fang, T. J. Wang, Super tough magnetic hydrogels for remotely triggered shape morphing, J. Mater. Chem. B 6 (2018) 2713–2722, https://doi.org/10.1039/c8tb00568k.

[22] A. Bhattacharyya, G. Janarthanan, I. Noh, Nano-biomaterials for designing functional bioinks towards complex tissue and organ regeneration in 3D bioprinting, Addit. Manuf. 37 (2021), 101639, https://doi.org/10.1016/j.addma.2020.101639.

[23] C. Li, J.P. Armstrong, I.J. Pence, W. Kit-Anan, J.L. Puetzer, S. Correia Carreira, A. C. Moore, M.M. Stevens, Glycosylated superparamagnetic nanoparticle gradients for osteochondral tissue engineering, Biomaterials 176 (2018) 24–33, https://doi.org/10.1016/j.biomaterials.2018.05.029.

[24] J. Penders, A.K. Rajasekharan, M. Hulander, M. Andersson, In situ gold nanoparticle gradient formation in a 3D meso- and macroporous polymer matrix, Macromol. Rapid Commun. 38 (2017) 1–5, https://doi.org/10.1002/marc.201700231.

[25] M.A. Skylar-Scott, J. Mueller, C.W. Visser, J.A. Lewis, Voxelated soft matter via multimaterial multinozzle 3D printing, Nature 575 (2019) 330–335, https://doi.org/10.1038/s41586-019-1736-8.

[26] D. Kokkinis, M. Schaffner, A.R. Studart, Multimaterial magnetically assisted 3D printing of composite materials, Nat. Commun. 6 (2015), https://doi.org/10.1038/ncomms9643.

[27] Y. Xia, Y. He, F. Zhang, Y. Liu, J. Leng, A review of shape memory polymers and composites: mechanisms, materials, and applications, Adv. Mater. 33 (2021), 2000713, https://doi.org/10.1002/adma.202000713.

[28] C. Yang, J. Luo, M. Polunas, N. Bosnjak, S.-T.D. Chueng, M. Chadwick, H. E. Sabaawy, S.A. Chester, K.-B. Lee, H. Lee, 4D-printed transformable tube array for high-throughput 3D cell culture and histology, Adv. Mater. 32 (2020), 2004285, https://doi.org/10.1002/adma.202004285.

[29] M. Champeau, D.A. Heinze, T.N. Viana, E.R. de Souza, A.C. Chinellato, S. Titotto, 4D printing of hydrogels: a review, Adv. Funct. Mater. 30 (2020), 1910606, https://doi.org/10.1002/adfm.201910606.

[30] R.L. Truby, J.A. Lewis, Printing soft matter in three dimensions, Nature 540 (2016) 371–378, https://doi.org/10.1038/nature21003.

[31] Z. Ding, C. Yuan, X. Peng, T. Wang, H.J. Qi, M.L. Dunn, Direct 4D printing via active composite materials, Sci. Adv. 3 (2017), https://doi.org/10.1126/sciadv.1602890.

[32] G. Gao, Z. Wang, D. Xu, L. Wang, T. Xu, H. Zhang, J. Chen, J. Fu, Snap-buckling motivated controllable jumping of thermo-responsive hydrogel bilayers, ACS Appl. Mater. Interfaces 10 (2018) 41724–41731, https://doi.org/10.1021/acsami.8b16402.

[33] J.T. Pham, M. Paven, S. Wooh, T. Kajiya, H.-J. Butt, D. Vollmer, Spontaneous jumping, bouncing and trampolining of hydrogel drops on a heated plate, Nat. Commun. 8 (2017) 905, https://doi.org/10.1038/s41467-017-01010-8.

[34] S. Liang, Y. Tu, Q. Chen, W. Jia, W. Wang, L. Zhang, Microscopic hollow hydrogel springs, necklaces and ladders: a tubular robot as a potential vascular scavenger, Mater. Horiz. 6 (2019) 2135–2142, https://doi.org/10.1039/C9MH00793H.

[35] J. Liu, W. Xu, Z. Kuang, P. Dong, Y. Yao, H. Wu, A. Liu, F. Ye, Gradient porous PNIPAM-based hydrogel actuators with rapid response and flexibly controllable deformation, J. Mater. Chem. C 8 (2020) 12092–12099, https://doi.org/10.1039/D0TC00139B.

[36] L. Wang, Y. Liu, Y. Cheng, X. Cui, H. Lian, Y. Liang, F. Chen, H. Wang, W. Guo, H. Li, M. Zhu, H. Ihara, A bioinspired swimming and walking hydrogel driven by light-controlled local density, Adv. Sci. 2 (2015), 1500084, https://doi.org/10.1002/advs.201500084.

[37] Y. Zhao, C. Xuan, X. Qian, Y. Alsaid, M. Hua, L. Jin, X. He, Soft phototactic swimmer based on self-sustained hydrogel oscillator, Sci. Robot 4 (2019) eaax7112, https://doi.org/10.1126/scirobotics.aax7112.

[38] W. Zhu, J. Li, Y.J. Leong, I. Rozen, X. Qu, R. Dong, Z. Wu, W. Gao, P.H. Chung, J. Wang, S. Chen, 3D-printed artificial microfish, Adv. Mater. 27 (2015) 4411–4417, https://doi.org/10.1002/adma.201501372.

[39] D. Podstawczyk, M. Nizioł, P. Szymczyk-Ziółkowska, M. Fiedot-Toboła, Development of thermoinks for 4D direct printing of temperature-induced self-rolling hydrogel actuators, Adv. Funct. Mater. 31 (2021), 2009664, https://doi.org/10.1002/adfm.202009664.

[40] S. Tottori, L. Zhang, F. Qiu, K.K. Krawczyk, A. Franco-Obregón, B.J. Nelson, Magnetic helical micromachines: fabrication, controlled swimming, and cargo transport, Adv. Mater. 24 (2012) 811–816, https://doi.org/10.1002/adma.201103818.

[41] S.-L. Xiang, Y.-X. Su, H. Yin, C. Li, M.-Q. Zhu, Visible-light-driven isotropic hydrogels as anisotropic underwater actuators, Nano Energy 85 (2021), 105965, https://doi.org/10.1016/j.nanoen.2021.105965.

[42] G. Qi, C. Zhe, C. Jianxiang, Z. Biao, Z. Yuan-Fang, L. Honggeng, H. Xiangnan, Y. Chao, L. Ji, M. Shlomo, Q. Shaoxing, 3D printing of highly stretchable hydrogel with diverse UV curable polymers, Sci. Adv. 7 (2021) eaba4261, https://doi.org/10.1126/sciadv.aba4261.

[43] K. Xiao, W. Jiangtao, C. Kaijuan, Z. Zeang, D. Zhen, H. Fengjingyang, F. Daining, Q. H. Jerry, Grayscale digital light processing 3D printing for highly functionally graded materials, Sci. Adv. 5 (2021) eaav5790, https://doi.org/10.1126/sciadv.aav5790.

[44] X. Tianqi, Z. Jiachen, S. Mohammad, O. Onaizah, D. Eric, Millimeter-scale flexible robots with programmable three-dimensional magnetization and motions, Sci. Robot. 4 (2019) eaav4494, https://doi.org/10.1126/scirobotics.aav4494.

[45] Z. Ji, C. Yan, B. Yu, X. Wang, F. Zhou, Multimaterials 3D printing for free assembly manufacturing of magnetic driving soft actuator, Adv. Mater. Interfaces 4 (2017), 1700629, https://doi.org/10.1002/admi.201700629.

[46] K. Tian, J. Bae, S.E. Bakarich, C. Yang, R.D. Gately, G.M. Spinks, M. in het Panhuis, Z. Suo, J.J. Vlassak, 3D printing of transparent and conductive heterogeneous hydrogel–elastomer systems, Adv. Mater. 29 (2017), 1604827, https://doi.org/10.1002/adma.201604827.

[47] K.K. Moncal, H. Gudapati, K.P. Godzik, D.N. Heo, Y. Kang, E. Rizk, D.J. Ravnic, H. Wee, D.F. Pepley, V. Ozbolat, G.S. Lewis, J.Z. Moore, R.R. Driskell, T.D. Samson, I.T. Ozbolat, Intra-operative bioprinting of hard, soft, and hard/soft composite tissues for craniomaxillofacial reconstruction, Adv. Funct. Mater. 31 (2021), 2010858, https://doi.org/10.1002/adfm.202010858.

[48] C. de Marco, S. Pané, B.J. Nelson, 4D printing and robotics, Sci. Robot. 3 (2018) eaau0449, https://doi.org/10.1126/scirobotics.aau0449.

[49] J.J. Schwartz, A.J. Boydston, Multimaterial actinic spatial control 3D and 4D printing, Nat. Commun. 10 (2019) 791, https://doi.org/10.1038/s41467-019-08639-7.

[50] C. Yuan, F. Wang, Q. Ge, Multimaterial direct 4D printing of high stiffness structures with large bending curvature, Extrem. Mech. Lett. 42 (2021), 101122, https://doi.org/10.1016/j.eml.2020.101122.

[51] B. Narupai, P.T. Smith, A. Nelson, 4D printing of multi-stimuli responsive protein-based hydrogels for autonomous shape transformations, Adv. Funct. Mater. 31 (2021), 2011012, https://doi.org/10.1002/adfm.202011012.

[52] R. Tognato, A.R. Armiento, V. Bonfrate, R. Levato, J. Malda, M. Alini, D. Eglin, G. Giancane, T. Serra, A stimuli-responsive nanocomposite for 3D anisotropic cell-guidance and magnetic soft robotics, Adv. Funct. Mater. 29 (2019), 1804647, https://doi.org/10.1002/adfm.201804647.

[53] D. Podstawczyk, M. Nizioł, P. Szymczyk, P. Wiśniewski, A. Guiseppi-Elie, 3D printed stimuli-responsive magnetic nanoparticle embedded alginate-methylcellulose hydrogel actuators, Addit. Manuf. 34 (2020), 101275, https://doi.org/10.1016/j.addma.2020.101275.

[54] Z. Chen, D. Zhao, B. Liu, G. Nian, X. Li, J. Yin, S. Qu, W. Yang, 3D printing of multifunctional hydrogels, Adv. Funct. Mater. 29 (2019), 1900971, https://doi.org/10.1002/adfm.201900971.

[55] D. Nuvoli, V. Alzari, J.A. Pojman, V. Sanna, A. Ruiu, D. Sanna, G. Malucelli, A. Mariani, Synthesis and characterization of functionally gradient materials obtained by frontal polymerization, ACS Appl. Mater. Interfaces 7 (2015) 3600–3606, https://doi.org/10.1021/am507725k.

[56] I.M. El-Galy, B.I. Saleh, M.H. Ahmed, Functionally graded materials classifications and development trends from industrial point of view, SN Appl. Sci. 1 (2019) 1378, https://doi.org/10.1007/s42452-019-1413-4.

[57] A. Ghosh, C. Yoon, F. Ongaro, S. Scheggi, F.M. Selaru, S. Misra, D.H. Gracias, Stimuli-responsive soft untethered grippers for drug delivery and robotic surgery, Front. Mech. Eng. 3 (2017) 7.

[58] J. Kim, S.E. Chung, S.-E. Choi, H. Lee, J. Kim, S. Kwon, Programming magnetic anisotropy in polymeric microactuators, Nat. Mater. 10 (2011) 747–752, https://doi.org/10.1038/nmat3090.

[59] W. Hu, G.Z. Lum, M. Mastrangeli, M. Sitti, Small-scale soft-bodied robot with multimodal locomotion, Nature 554 (2018) 81–85, https://doi.org/10.1038/nature25443.

[60] C. Ravikumar, R. Bandyopadhyaya, Mechanistic study on magnetite nanoparticle formation by thermal decomposition and coprecipitation routes, J. Phys. Chem. C 115 (2011) 1380–1387, https://doi.org/10.1021/jp105304w.

[61] K. Schütz, A.M. Placht, B. Paul, S. Brüggemeier, M. Gelinsky, A. Lode, Three-dimensional plotting of a cell-laden alginate/methylcellulose blend: towards biofabrication of tissue engineering constructs with clinically relevant dimensions, J. Tissue Eng. Regen. Med. 11 (2017) 1574–1587, https://doi.org/10.1002/term.2058.

[62] H. Li, Y.J. Tan, K.F. Leong, L. Li, 3D bioprinting of highly thixotropic alginate/methylcellulose hydrogel with strong interface bonding, ACS Appl. Mater. Interfaces 9 (2017) 20086–20097, https://doi.org/10.1021/acsami.7b04216.

[63] H.-R. Lin, L.-H. Ou, Y.-J. Lin, M.-H. Ling, Hollow, pH-sensitive calcium–alginate/poly(acrylic acid) hydrogel beads as drug carriers for vancomycin release, J. Appl. Polym. Sci. 118 (2010) 1878–1886, https://doi.org/10.1002/app.32574.

[64] Z. Zhou, X. Zhu, D. Wu, Q. Chen, D. Huang, C. Sun, J. Xin, K. Ni, J. Gao, Anisotropic shaped iron oxide nanostructures: controlled synthesis and proton relaxation shortening effects, Chem. Mater. 27 (2015) 3505–3515, https://doi.org/10.1021/acs.chemmater.5b00944.

[65] M.-H. Hsiao, K.-H. Lin, D.-M. Liu, Improved pH-responsive amphiphilic carboxymethyl-hexanoyl chitosan–poly(acrylic acid) macromolecules for biomedical applications, Soft Matter 9 (2013) 2458–2466, https://doi.org/10.1039/C2SM27610K.

[66] Q. Ju, W. Luo, Y. Liu, H. Zhu, R. Li, X. Chen, Poly (acrylic acid)-capped lanthanide-doped BaFCl nanocrystals: synthesis and optical properties, Nanoscale 2 (2010) 1208–1212, https://doi.org/10.1039/C0NR00116C.

[67] A. Pardo, M. Gómez-Florit, S. Barbosa, P. Taboada, R.M.A. Domingues, M. E. Gomes, Magnetic nanocomposite hydrogels for tissue engineering: design concepts and remote actuation strategies to control cell fate, ACS Nano 15 (2021) 175–209, https://doi.org/10.1021/acsnano.0c08253.

[68] T. Ahlfeld, V. Guduric, S. Duin, A.R. Akkineni, K. Schütz, D. Kilian, J. Emmermacher, N. Cubo-Mateo, S. Dani, M. v Witzleben, J. Spangenberg, R. Abdelgaber, R.F. Richter, A. Lode, M. Gelinsky, Methylcellulose – a versatile printing material that enables biofabrication of tissue equivalents with high shape fidelity, Biomater. Sci. 8 (2020) 2102–2110, https://doi.org/10.1039/D0BM00027B.

[69] M.C. Arno, M. Inam, A.C. Weems, Z. Li, A.L.A. Binch, C.I. Platt, S.M. Richardson, J. A. Hoyland, A.P. Dove, R.K. O'Reilly, Exploiting the role of nanoparticle shape in enhancing hydrogel adhesive and mechanical properties, Nat. Commun. 11 (2020) 1420, https://doi.org/10.1038/s41467-020-15206-y.

[70] K. Markstedt, A. Mantas, I. Tournier, H. Martínez Ávila, D. Hägg, P. Gatenholm, 3D bioprinting human chondrocytes with nanocellulose–alginate bioink for cartilage tissue engineering applications, Biomacromolecules 16 (2015) 1489–1496, https://doi.org/10.1021/acs.biomac.5b00188.

[71] K. Sonnleitner, C. Huber, I. Teliban, S. Kobe, B. Saje, D. Kagerbauer, M. Reissner, C. Lengauer, M. Groenefeld, D. Suess, 3D printing of polymer-bonded anisotropic

magnets in an external magnetic field and by a modified production process, Appl. Phys. Lett. 116 (2020) 92403, https://doi.org/10.1063/1.5142692.
[72] B.G. Compton, J.W. Kemp, T.V. Novikov, R.C. Pack, C.I. Nlebedim, C.E. Duty, O. Rios, M.P. Paranthaman, Direct-write 3D printing of NdFeB bonded magnets, Mater. Manuf. Process. 33 (2018) 109–113, https://doi.org/10.1080/10426914.2016.1221097.
[73] J. Wang, Y. Liu, X. Zhang, S.E. Rahman, S. Su, J. Wei, F. Ning, Z. Hu, R. Martínez-Zaguilán, S.R. Sennoune, W. Cong, G. Christopher, K. Zhang, J. Qiu, 3D printed agar/ calcium alginate hydrogels with high shape fidelity and tailorable mechanical properties, Polymer 214 (2021), 123238, https://doi.org/10.1016/j.polymer.2020.123238.
[74] M. Filippi, B. Dasen, J. Guerrero, F. Garello, G. Isu, G. Born, M. Ehrbar, I. Martin, A. Scherberich, Magnetic nanocomposite hydrogels and static magnetic field stimulate the osteoblastic and vasculogenic profile of adipose-derived cells, Biomaterials 223 (2019), 119468, https://doi.org/10.1016/j.biomaterials.2019.119468.
[75] M.S. Islam, T.G. Molley, J. Ireland, J.J. Kruzic, K.A. Kilian, Magnetic nanocomposite hydrogels for directing myofibroblast activity in adipose-derived stem cells, Adv. NanoBiomed Res. 1 (2021), 2000072, https://doi.org/10.1002/anbr.202000072.
[76] Y. Li, G. Huang, X. Zhang, B. Li, Y. Chen, T. Lu, T.J. Lu, F. Xu, Magnetic hydrogels and their potential biomedical applications, Adv. Funct. Mater. 23 (2013) 660–672, https://doi.org/10.1002/adfm.201201708.
[77] J. Spangenberg, D. Kilian, C. Czichy, T. Ahlfeld, A. Lode, S. Günther, S. Odenbach, M. Gelinsky, Bioprinting of magnetically deformable scaffolds, ACS Biomater. Sci. Eng. 7 (2021) 648–662, https://doi.org/10.1021/acsbiomaterials.0c01371.
[78] A. Amore Bonapasta, F. Buda, P. Colombet, Interaction between Ca ions and poly (acrylic acid) chains in macro-defect-free cements: a theoretical study, Chem. Mater. 13 (2001) 64–70, https://doi.org/10.1021/cm000505o.
[79] L.M. Fuhrer, S. Sun, V. Boyko, M. Kellermeier, H. Cölfen, Tuning the properties of hydrogels made from poly(acrylic acid) and calcium salts, Phys. Chem. Chem. Phys. 22 (2020) 18631–18638, https://doi.org/10.1039/D0CP02649B.
[80] Y. Sapir, B. Polyak, S. Cohen, Cardiac tissue engineering in magnetically actuated scaffolds, Nanotechnology 25 (2014), https://doi.org/10.1088/0957-4484/25/1/014009.
[81] R.I. Baron, G. Biliuta, V. Socoliuc, S. Coseri, Affordable magnetic hydrogels prepared from biocompatible and biodegradable sources, Polymer 13 (2021) 1693, https://doi.org/10.3390/polym13111693.
[82] S. Naghieh, M.R. Karamooz-Ravari, M.D. Sarker, E. Karki, X. Chen, Influence of crosslinking on the mechanical behavior of 3D printed alginate scaffolds: experimental and numerical approaches, J. Mech. Behav. Biomed. Mater. 80 (2018) 111–118, https://doi.org/10.1016/j.jmbbm.2018.01.034.
[83] J. Jang, Y.-J. Seol, H.J. Kim, J. Kundu, S.W. Kim, D.-W. Cho, Effects of alginate hydrogel cross-linking density on mechanical and biological behaviors for tissue engineering, J. Mech. Behav. Biomed. Mater. 37 (2014) 69–77, https://doi.org/10.1016/j.jmbbm.2014.05.004.
[84] V. Kshirsagar, S. Tchessalov, F. Kanka, D. Hiebert, A. Alexeenko, Determining maximum sublimation rate for a production lyophilizer: computational modeling and comparison with ice slab tests, J. Pharm. Sci. 108 (2019) 382–390, https://doi.org/10.1016/j.xphs.2018.10.061.
[85] A. Spinnrock, D. Schupp, H. Cölfen, Nanoparticle gradient materials by centrifugation, Small 14 (2018), 1803518, https://doi.org/10.1002/smll.201803518.
[86] W. Shi, J. Huang, R. Fang, M. Liu, Imparting functionality to the hydrogel by magnetic-field-induced nano-assembly and macro-response, ACS Appl. Mater. Interfaces 12 (2020) 5177–5194, https://doi.org/10.1021/acsami.9b16770.